

# CHARACTERISTICS OF VLF SAUCERS AND AURORAL HISSES FROM ISIS SATELLITES RECEIVED AT SYOWA STATION, ANTARCTICA

Tadanori ONDOH, Yoshikatsu NAKAMURA and Toshimitsu MURAKAMI

*Radio Research Laboratories, 2-1, Nukui-Kitamachi  
4-chome, Koganei-shi, Tokyo 184*

**Abstract:** Properties of VLF saucers and auroral hisses have been studied by using ISIS VLF electric field data (50 Hz–30 kHz) received at Syowa Station, Antarctica. Source altitudes of VLF saucers are obtained from frequency-time spectra of VLF saucers by assuming the limiting ray model. The source distances of VLF saucers are less than about 800 km below the satellite. VLF saucers occur around the high- and low-latitude ends of the auroral hiss region.

The active auroral hiss and the stable auroral hiss are classified according to the variability of the narrow-band intensity data processed from ISIS VLF tapes. The frequent occurrence region of the former agrees well with the usual auroral zone, while the latter occurs at invariant latitude from about 70° to about 80° both on the day and night sides. The properties of the stable auroral hiss have some similarities to those of the precipitating low-energy electrons, the so-called polar rain, in occurrence region and in intensity.

The narrow-band 5 kHz hiss occurs often at invariant latitudes of  $61^\circ \pm 5^\circ$ , which are close to the average plasmapause latitude, during the daytime and nighttime.

## 1. Introduction

MOSIER and GURNETT (1969) found saucer-shaped emissions by the low-altitude satellite Injun-5 and they detected by the measurement of the VLF wave Poynting flux that VLF saucers propagated from below the Injun-5. The  $f$ - $t$  spectra of VLF saucers have been explained by the limiting rays emitted from the radio source below the satellite altitude (MOSIER and GURNETT, 1969). JAMES (1976) has explained the VLF saucer by the incoherent Cerenkov radiation emitted from upward electrons with energy less than 5 eV.

However, the source altitudes of the VLF saucers have not yet been actually known. We will obtain source altitudes of the VLF saucers from  $f$ - $t$  spectra of VLF saucers observed by ISIS satellites using the limiting ray models derived by MOSIER and GURNETT (1969) and TEMERIN (1979).

The spatial distribution of the auroral hiss over the polar region has been studied from the  $f$ - $t$  spectra of VLF emissions observed by the low altitude satellites (TAYLOR and GURNETT, 1968; HUGHES *et al.*, 1971), and electromagnetic plasma wave emis-

sions from the auroral field lines have been extensively reviewed by GURNETT (1978). But the spatial variation of the auroral hiss intensity can not be well examined by the  $f$ - $t$  spectrum data because the intensity range of light and shade of the VLF spectrum films is at most about 10 dB. In this paper, the narrow-band intensity vs. time (or latitude) data at 20 kHz, 16 kHz, 8 kHz, 5 kHz, 1.5 kHz and 300 Hz are analyzed to obtain large-scale features of the intensity variation of auroral VLF emissions over the polar region.

Finally, the narrow band 5 kHz hisses have been frequently found around the invariant latitude of  $61^\circ$  from ISIS VLF data received at Syowa Station, Antarctica, and the origin of the narrow band 5 kHz will be discussed in terms of the wave particle interactions.

## 2. Source Altitudes of VLF Saucers

MOSIER and GURNETT (1969) have reported from the Poynting flux measurements of the VLF saucers that VLF saucers propagate upward from below the satellite. They have also explained the  $f$ - $t$  spectra of VLF saucers by the limiting ray model from the radio sources below the satellite. The limiting ray angle to the geomagnetic field,  $\psi_{\text{res}} = \pi/2 - \theta_{\text{res}}$  is given by  $\cot^2 \psi_{\text{res}} = -(P/S) = \tan^2 \theta_{\text{res}}$  (STIX, 1962) where  $\theta_{\text{res}}$  denotes the resonance cone angle. The limiting ray angle to the geomagnetic field increases with increasing frequency, hence it can explain the saucer-shaped spectrum.

If  $x$  is the horizontal distance (also proportional to the time coordinate on the spectrogram) from the symmetry axis of the emission and  $h$  is the altitude of the satellite above the source, then

$$(x/h)^2 = \tan^2 \psi_{\text{res}} = (-S/P). \quad (1)$$

The minimum frequency of the emission envelope ( $x=0$ ) is the lower-hybrid-resonance (LHR) frequency, where  $S=0$  (MOSIER and GURNETT, 1969). From the above eq. (1), the equation for the frequency of the VLF saucer as a function of distance is given for

$$f_p^2 \gg f^2 \text{ and } f_H \gg f \text{ by } f^2 = \alpha^2 \cdot (x/h)^2 + f_{\text{LHR}}^2, \quad (2)$$

$$f_{\text{LHR}}^2 = \alpha^2 \cdot (m_e/m_p) \cdot \frac{1}{m_1(\text{eff})} \quad (3)$$

and

$$\alpha^2 = \frac{f_H^2 \cdot f_p^2}{f_H^2 + f_p^2}$$

where  $h$  is the distance between the source and the satellite,  $m_1(\text{eff})$  the harmonic mean mass number of all positive ions in the medium,  $f_H$  the electron gyro-frequency,

$f_p$  the electron plasma frequency,  $m_e$  the electron mass, and  $m_p$  the proton mass. If  $\Delta t$  is the time interval between the two traces of a VLF saucer on the spectrogram, and  $v$  is the average satellite velocity computed from orbit data, we have  $2x = v \cdot \Delta t$ , where  $v$  ranges from 7.3 km/s to 5.8 km/s. The latitudinal distribution of the har-

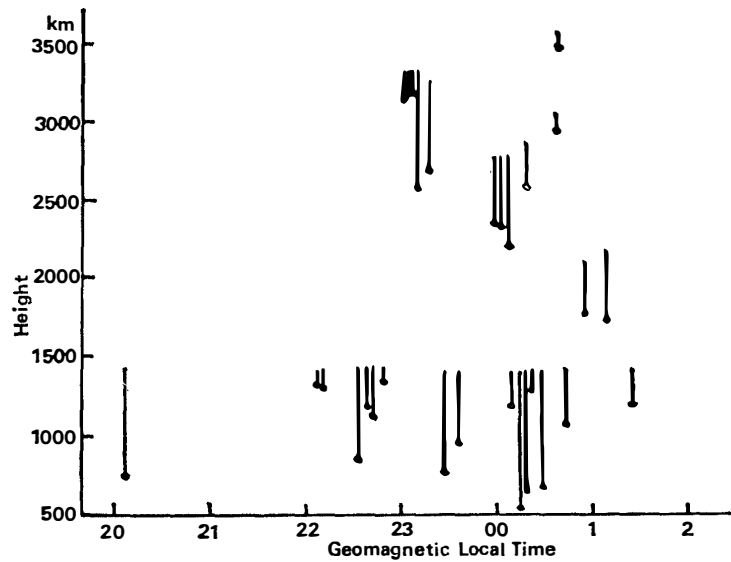


Fig. 1. Local-time distributions of source altitudes of VLF saucers estimated by the limiting ray model and receiving-point (ISIS-1 or ISIS-2) altitudes, where the upper ends of rods show the satellite altitudes and the bottom solid circles of rods show the source altitudes of VLF saucers estimated.

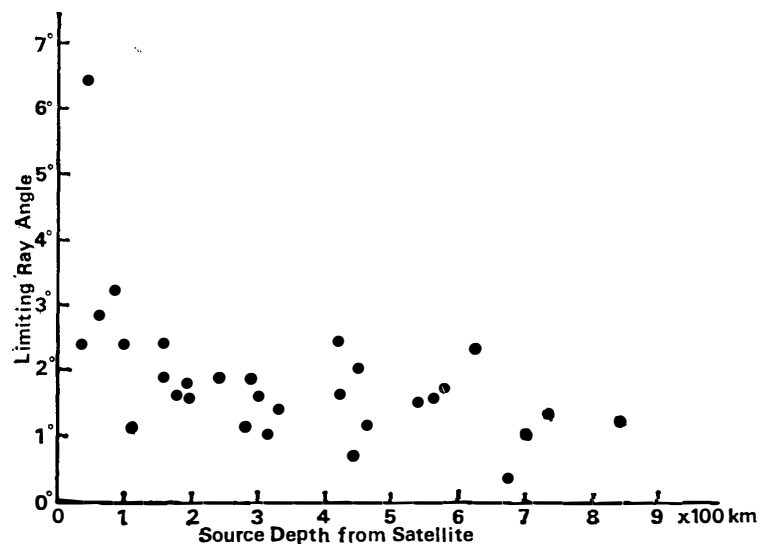


Fig. 2. Relation between limiting ray angles of VLF saucers and saucer source depth from the satellite.

monic mean ion mass number obtained from the LHR hiss (BARRINGTON, 1969) shows the average value of  $m_i(\text{eff}) = 11$  in the auroral-zone and the polar topside ionosphere. We can determine  $\alpha^2$  by using  $m_i(\text{eff}) = 11$  and the relation of eq. (3).

Finally, we have the source distance,  $h$  below the satellite by substituting measured values of  $f$ ,  $x (= v \cdot \Delta t / 2)$  and  $f_{\text{LHR}}$  into the eq. (2).

Fig. 1 shows the relation of the geomagnetic local time of the saucer occurrence vs. altitudes of the satellite and of source positions of the VLF saucers estimated above. This indicates that the propagation distances between VLF saucers and the satellites are less than about 800 km. This means that VLF saucers occur relatively near the satellite. In Fig. 1, solid circles at the bottom of rods show estimated sources of the VLF saucers and upper ends of the rods show the altitudes of ISIS-1 or ISIS-2.

Furthermore, we can obtain the limiting ray angles of VLF saucers to the geomagnetic field line from  $(x/h)^2 = \tan^2 \psi_{\text{res}}$ . Fig. 2 illustrates the relation between the source distance of VLF saucers from the satellite and the limiting ray angles. The limiting ray angle seems to increase with decreasing source distance from the satellite, although  $\psi_{\text{res}}$  depends on  $x$ ,  $h$  and  $f$  as indicated by the expression of eqs. (1) and (2).

Most limiting ray angles,  $\psi_{\text{res}}$  in Fig. 2 are below  $3.5^\circ$ . In other words, the wave normal angles of VLF saucers received at the satellite are very large as  $\theta_{\text{res}} = \pi/2 - \psi_{\text{res}}$ . This is consistent with the result of Fig. 1 that the VLF saucers occur near the satellite. The VLF saucer will still have large wave normal angles after a relatively short-distance propagation because the VLF saucer is originally emitted at large wave normal angles nearly perpendicular to the geomagnetic field by the Cerenkov radiation.

In this paper, the narrow-band intensity vs. time (latitude) data at the six frequencies are processed from the wide-band magnetic tapes of ISIS VLF data received at Syowa Station (geomag. lat.  $69.7^\circ\text{S}$ , long.  $77.7^\circ\text{E}$ ), Antarctica by using narrow-band DC amplifiers with a minimum reading circuit of a charging time constant of 10 s and a discharging time constant of 10 ms. The narrow-band intensity data show more detailed structure of VLF emissions than the  $f$ - $t$  spectrum films because the intensity range of light and shade of the VLF spectrum films is at most 10 dB. The intensity scale of the narrow band data is in arbitrary unit, because the ISIS VLF electric field data are regulated by the automatic gain control.

Fig. 3a shows typical examples of VLF saucers observed at invariant latitudes of  $72^\circ$  and  $68.6^\circ$  at  $Kp = 1 -$ . Fig. 3b is the corresponding narrow-band intensity data at 20 kHz, 16 kHz, 8 kHz, 5 kHz, 1.5 kHz and 300 Hz observed on June 6, 1977. In Fig. 3b, the VLF saucers are clearly seen as two-peak intensity variations at 8 kHz and 5 kHz bands as shown by downward triangles, and VLF saucers occur near the high- and low-latitude ends of the auroral hiss zone. Figs. 4a and 4b illustrate the frequency-time spectra and corresponding narrow-band data of the VLF saucers observed on July 12, 1977 over the polar-cap region at  $Kp = 0 +$ . Downward triangles in Fig. 4b show that VLF saucers occur around the high-latitude end (invariant

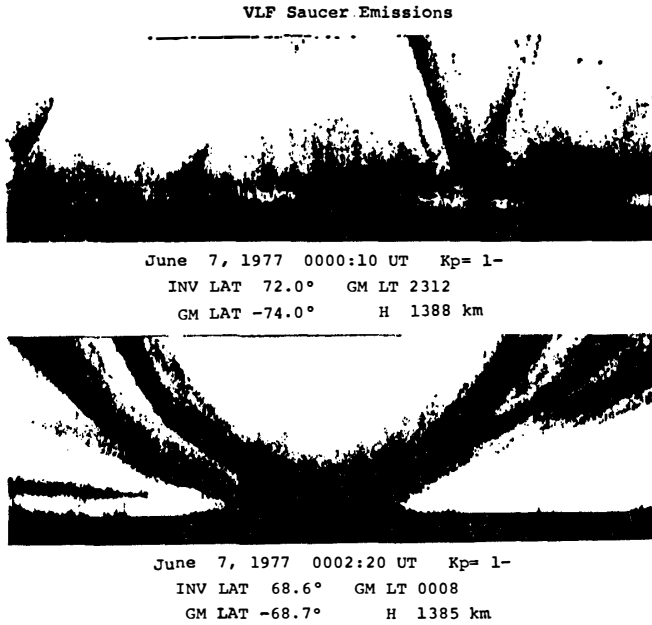


Fig. 3a. Typical spectra of VLF saucers observed by the ISIS-2 around the geomagnetic mid-night on June 7, 1977 ( $K_p=1-$ ) over the southern auroral zone. The full scale on ordinate is 10 kHz in frequency and the interval between white dots at bottom is one second. All VLF spectra given below have the same scale as the present ones in frequency and in time.

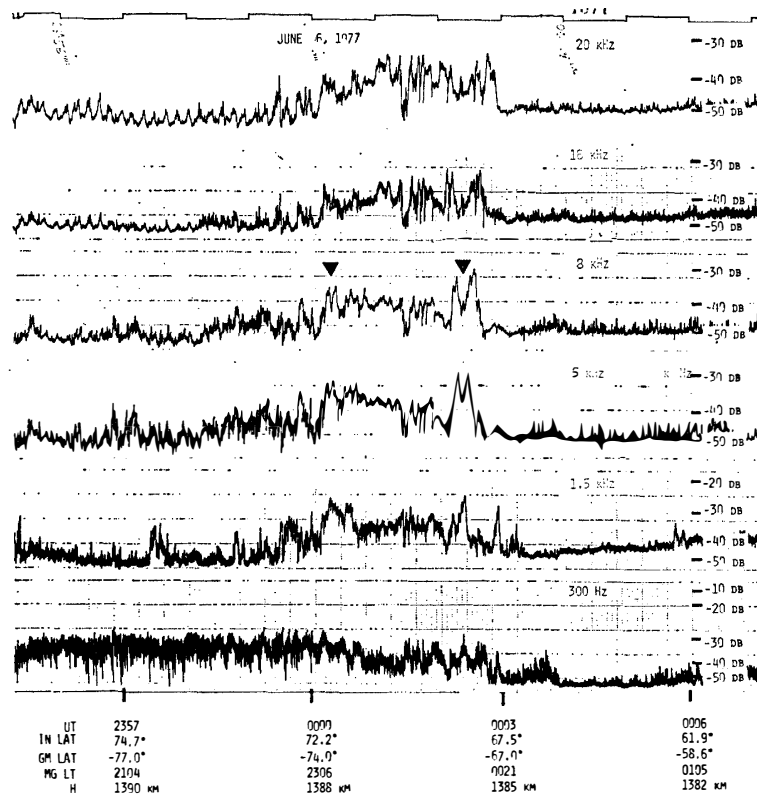


Fig. 3b. Narrow-band intensity data of the same ISIS pass as Fig. 3a, where downward triangles show the locations of VLF saucers in Fig. 3a.

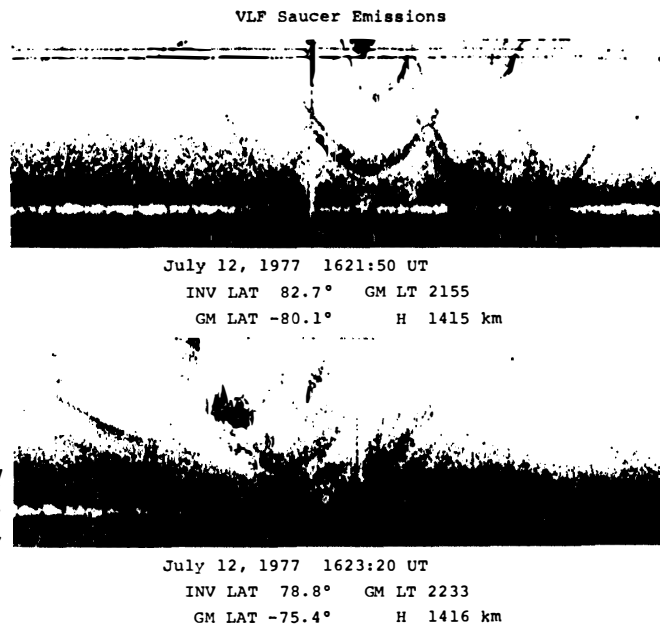


Fig. 4a. VLF saucer spectra observed around geomagnetic local time of 22 hours on July 12, 1977 ( $K_p=0+$ ) in the polar cap region.

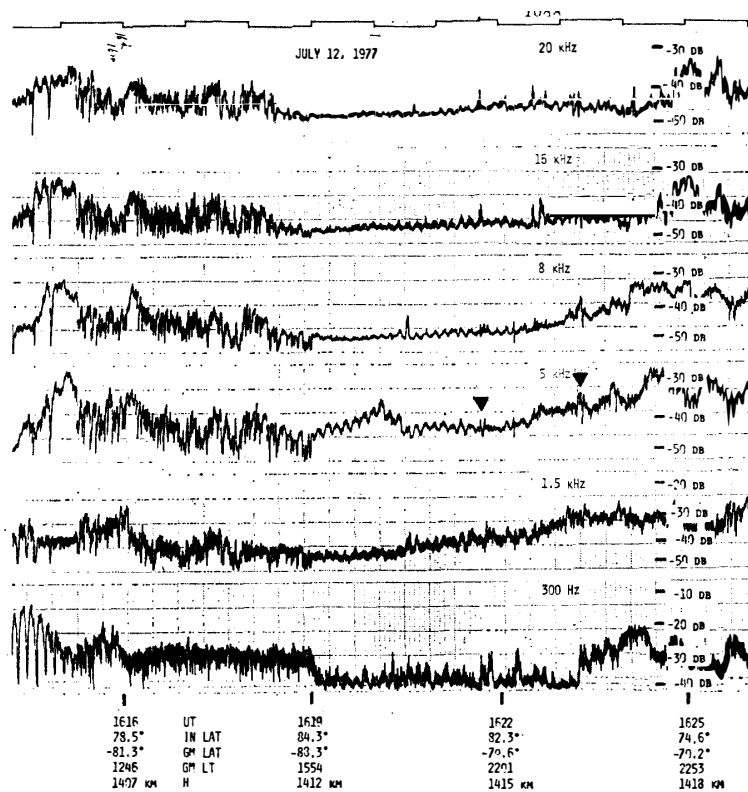


Fig. 4b. Narrow-band intensity data of the same ISIS-2 pass as Fig. 4a, where downward triangles show locations of VLF saucers in Fig. 4a.

latitude of  $82.7^\circ$  and  $78.8^\circ$ ) of the wide-band auroral hiss on the night side of the polar day-night pass, and that the electric field in the 300 Hz band is extremely low over the polar cap region both on the day and night sides. Thus, the VLF saucer seems to occur often in the vicinity of the high- and low-latitude ends of the wide-band auroral hiss in the nighttime though OZAKI *et al.* (1979) have concluded that the occurrence region of VLF saucers lies on the low-latitude side of the auroral hiss zone outside the plasmopause. But, we need more statistical studies of the VLF saucer before reaching the conclusion.

### 3. Polar Cusp Hiss

Figs. 5a and 5b also show a polar day-night pass observed on July 15, 1977 at  $Kp=3-$ . The upper panel of Fig. 5a illustrates structured or changeable characteristics (in time scale less than 10 s) of the auroral hiss observed in the daytime, while the lower panel illustrates a rather steady auroral hiss observed in the nighttime. The narrow-band data in Fig. 5b clearly show the difference of hiss characteristics between the day and night sides in time variation of the hiss intensity in frequency bands above 5 kHz, where the downward triangles indicate the location of VLF hiss spectra shown in Fig. 5a. An extremely low level of the 300 Hz band is seen on both the dayside and nightside of the polar cap region in Fig. 5b as well as Fig. 4b. Here we define

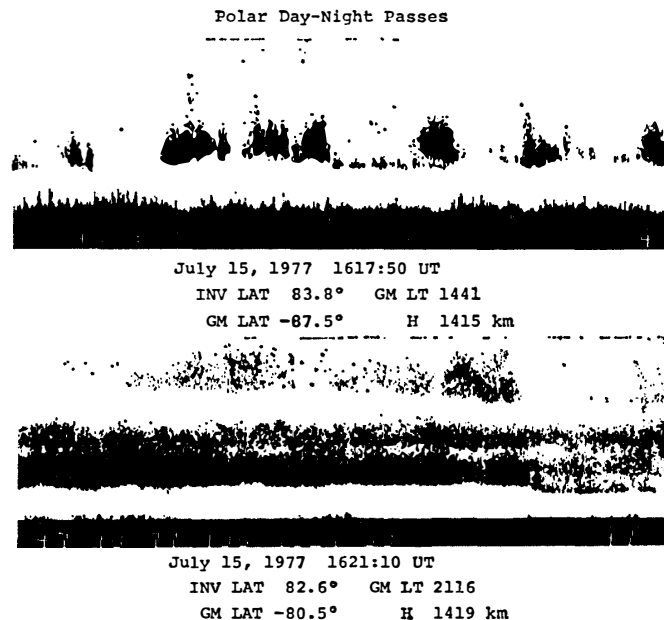


Fig. 5a. VLF spectra for ISIS-2 pass crossing the polar cap from the dayside to the nightside on July 15, 1977 ( $Kp=3-$ ). The upper panel shows changeable characteristics of the polar cusp hiss observed in the afternoon. The lower panel shows a uniform spectrum of the auroral hiss observed in the nighttime.

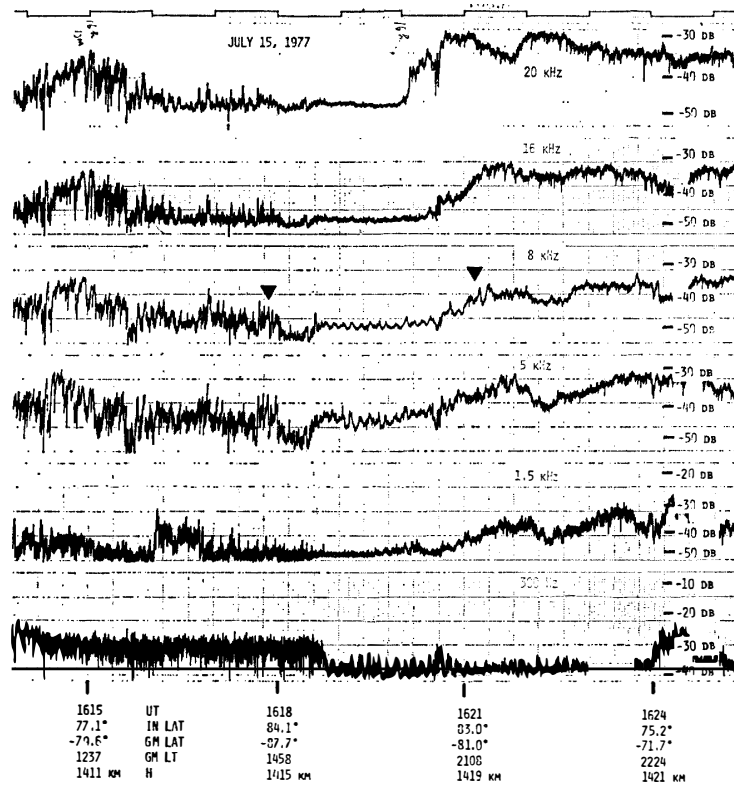


Fig. 5b. Narrow-band intensity data of the same ISIS pass as Fig. 5a, where downward triangles show locations of the VLF spectra in Fig. 5a. Remark the very low level of intensity for the 300 Hz band in the polar cap region.

the structured or changeable auroral hiss observed in the dayside polar-cap region as the polar cusp hiss.

Fig. 6a shows other examples of the polar cusp hisses observed on July 11, 1977 at  $Kp=3$  and on January 19, 1978 at  $Kp=2-$ . These VLF spectra have fine or changeable structure in frequency and in time scale less than 10 s. The polar cusp hiss usually occurs at frequencies above a few kHz as well as the auroral hiss in the nighttime. The downward triangle of Fig. 6b indicates the location of the polar-cusp hiss in the upper panel of Fig. 6a. The polar-cusp hiss of Fig. 6b occurs at invariant latitudes from about  $73^\circ$  to  $76^\circ$  in the morning hours and has fine intensity variations more than 10 dB within 10 s in frequency bands above 5 kHz. The two triangles of Fig. 6c also correspond to the middle and bottom panels of Fig. 6a. The polar cusp hiss on January 19, 1978 (Fig. 6c) observed at invariant latitudes for  $77^\circ$ – $83^\circ$  from the morning to the afternoon has also the same fine structures as that on July 11, 1977 in Fig. 6b.

The fine structured intensity or spectrum of the polar cusp hiss may be related to the structured flux of precipitated electrons with energies near 1 keV, the so-called

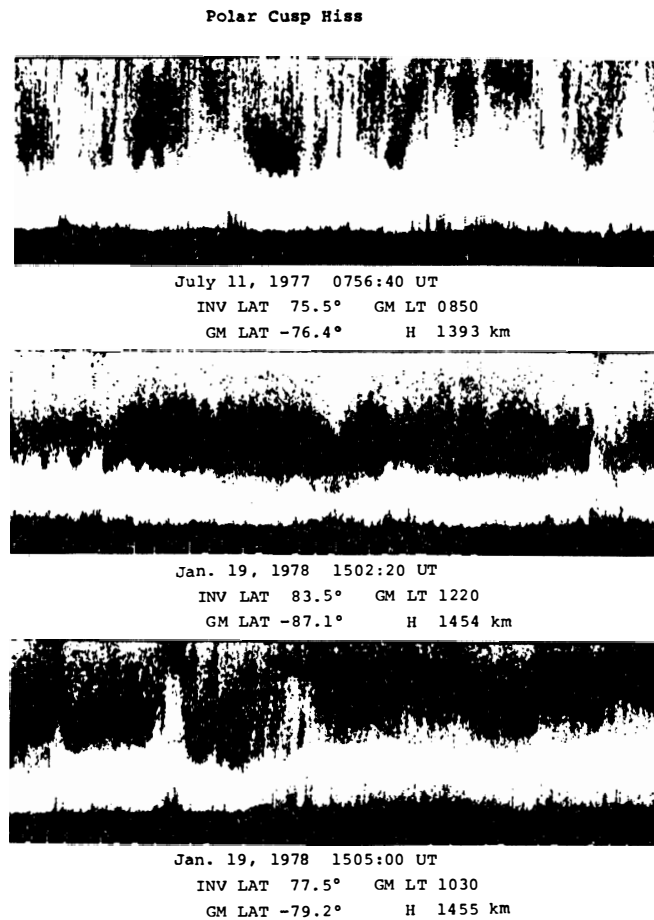


Fig. 6a. Typical spectra of polar cusp hisses observed in the dayside polar cap on July 11, 1977 ( $Kp=3$ ) and on January 19, 1978 ( $Kp=2-$ ) by the ISIS-2.

polar showers or the highly structured flux of electrons with energies near a few keV, the so-called polar squall (WINNINGHAM and HEIKKILA, 1974). Further study will be necessary to define the relation between the polar cusp hiss proposed here and the polar showers (or polar squall) or structured auroras in the polar cap region.

#### 4. New Property of the Auroral Hiss

Simultaneous observations of the auroral hiss by Injun-5 and of visual aurora along the same geomagnetic field line have shown good correlations between the wide-band auroral hiss and the discrete auroral arc (MOSIER and GURNETT, 1969). Also, detailed correlations have been found between the auroral hiss and an intense flux of the precipitating Inverted-V electrons with energies for 100 eV–1 keV (GURNETT, 1978).

The maximum occurrence of auroral hiss closely follows the auroral oval which

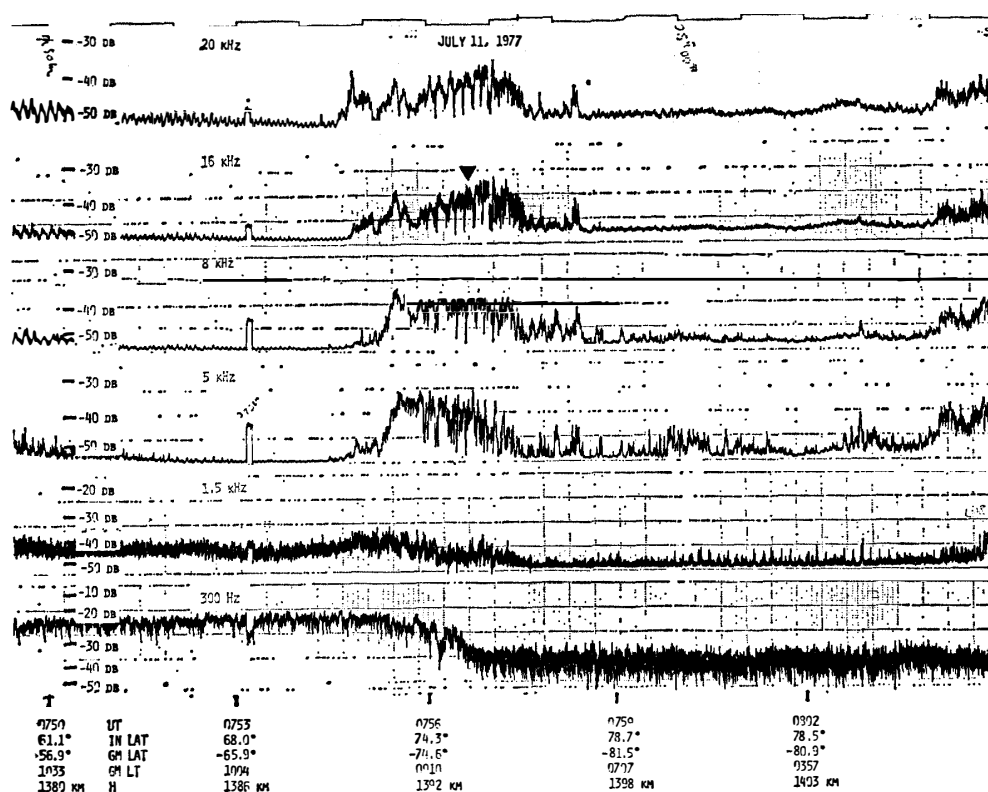


Fig. 6b. Narrow-band intensity data of the polar cusp hiss for the same ISIS pass as the upper panel of Fig. 6a on July 11, 1977 where a downward triangle shows the location of the polar cusp hiss in the upper panel.

varies from about  $80^\circ$  invariant latitude on the dayside to about  $72^\circ$  on the nightside. The diurnal variation of the auroral hiss occurrence has a pronounced dawn-dusk asymmetry with a distinct minimum from about 2 to 8 hour magnetic local time. This dawn-dusk asymmetry may be related to the dawn-dusk asymmetry in the spectrum and intensity of the precipitating auroral electrons (FRANK and ACKERSON, 1972; HUGHES *et al.*, 1971).

Since all the above studies on the auroral hiss are based on the  $f$ - $t$  spectrum data, we can not obtain the global morphology of the intensity variation of auroral hiss in the polar region. The narrow-band intensity data at the six frequencies are most suitable for this purpose as shown by Figs. 4b–6b.

Fig. 7 shows a wide-band auroral hiss observed for late night hours in magnetic local time on June 8, 1977 at  $Kp=2$ . The wide-band hiss in Fig. 7 appears in frequency bands above 5 kHz. The wide-band hiss occurring before 2321 UT at invariant latitudes above  $73^\circ$  has the stable and steady property in intensity variation, while the wide-band auroral hiss occurring between 2321 UT and 2327 UT shows an active and changeable property in intensity variation as well as the polar cusp hiss.

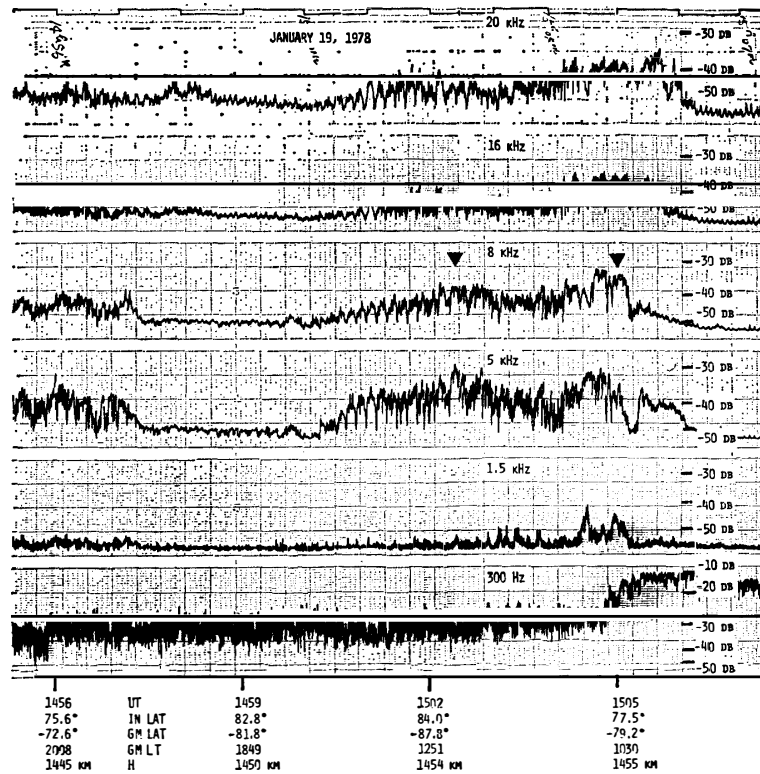


Fig. 6c. Narrow-band intensity data for the same ISIS pass as the middle and bottom panels of Fig. 6a on January 19, 1978, where downward triangles show locations of the VLF spectra in the middle and bottom panels in Fig. 6a.

For convenience, we classify the former and the latter hisses into the stable- and active-auroral hisses respectively only from the viewpoint of the morphological features in intensity variation of the auroral hiss. So, quantitatively the active auroral hiss must have an intensity variation greater than 3 dB for 10 s at frequency bands more than two of the narrow band intensity data.

The stable auroral hiss occurs usually on the high-latitude side of the active auroral hiss, and its intensity varies very little with latitude or time as shown by Fig. 7. However, the stable auroral hiss does not always occur together with the active auroral hiss.

Fig. 8 shows latitudinal distributions for the occurrence frequency of the active auroral hiss defined above during the daytime (06–18 magnetic local time) and the nighttime (18–06 magnetic local time). These distributions are derived from the narrow-band intensity data of the ISIS VLF electric field (50 Hz–30 kHz) received at Syowa Station, Antarctica (geomag. lat. 69.7°S, long. 77.7°E) from February 1977 to January 1978. The active auroral hiss occurs often in the latitudinal range from

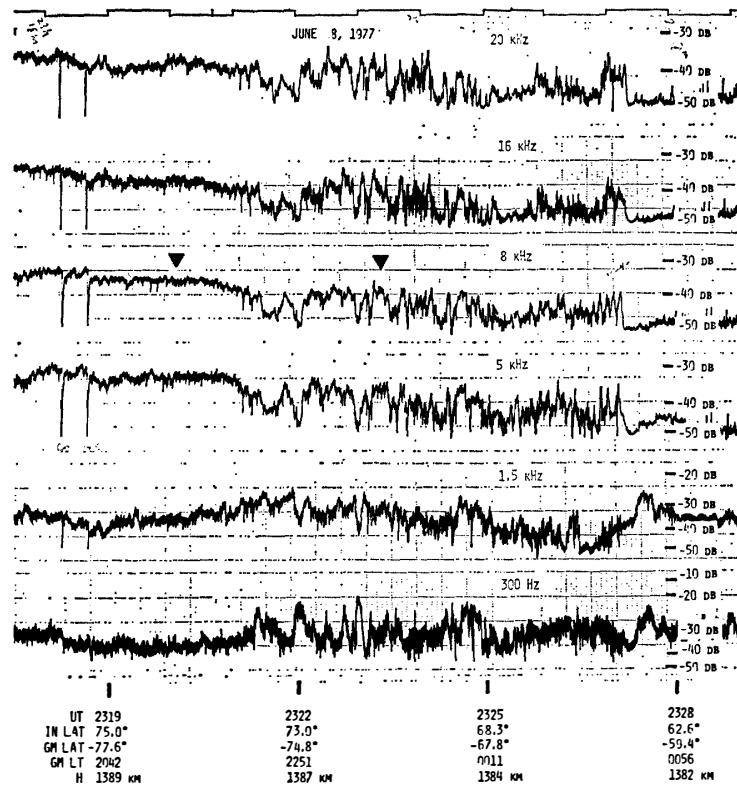


Fig. 7. Examples of the active auroral hiss and the stable auroral hiss as represented by the narrow-band intensity data which were received from ISIS-2 at Syowa Station, Antarctica on June 8, 1977 ( $K_p=2$ ). The stable auroral hiss occurs at invariant latitudes above  $73^\circ$  and the active auroral hiss occurs between  $73^\circ$  and  $63^\circ$ .

about  $65^\circ$  to about  $75^\circ$  on the nightside, and it occurs often in the latitudinal range from about  $73^\circ$  to about  $83^\circ$  on the dayside.

Figs. 9 and 10 show latitudinal distributions of the occurrence frequency of the stable auroral hiss for  $K_p \leq 3$  and for  $K_p > 3$  respectively. These distributions are also derived from narrow-band intensity data of the ISIS VLF electric field which were received at Syowa Station, Antarctica from February 1977 to January 1978. For  $K_p \leq 3$  (Fig. 9), the stable auroral hiss occurs frequently at invariant latitudes of  $68^\circ$ – $77^\circ$  on the nightside (18–06 MLT) and at latitudes of  $70^\circ$ – $80^\circ$  on the dayside (06–18 MLT) respectively. For  $K_p > 3$  (Fig. 10), the stable auroral hiss occurs at invariant latitudes of about  $68^\circ$ – $77^\circ$  on the nightside and at latitude of about  $70^\circ$ – $79^\circ$  on the dayside although the number of data used is not many in the case of the dayside for  $K_p > 3$ . Hence, the general features of the occurrence frequency of the stable auroral hiss for  $K_p \leq 3$  are almost the same as those for  $K_p > 3$ , and the stable auroral hiss zone in latitude is approximately the same for the dayside and nightside.

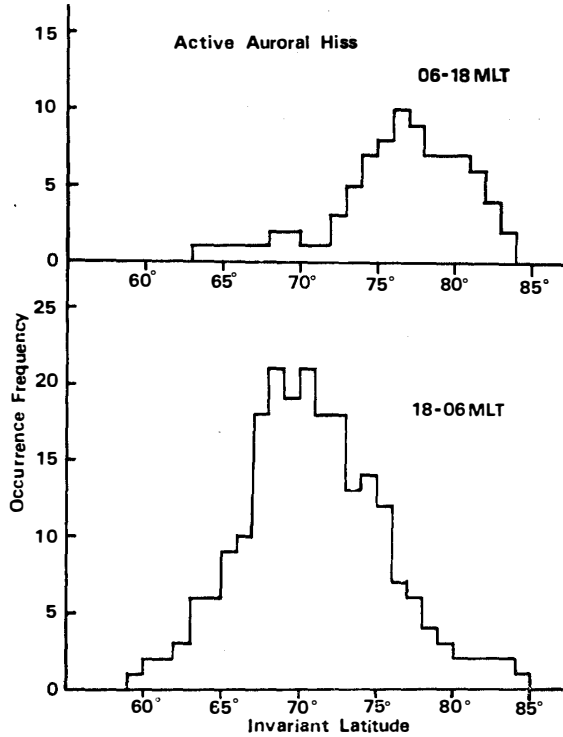


Fig. 8. Latitudinal distributions of the occurrence frequency of the active auroral hiss in the daytime (06–18 MLT) and in the nighttime (18–06 MLT). The VLF data used were received from ISIS satellites at Syowa Station, Antarctica from January 1977 to February 1978.

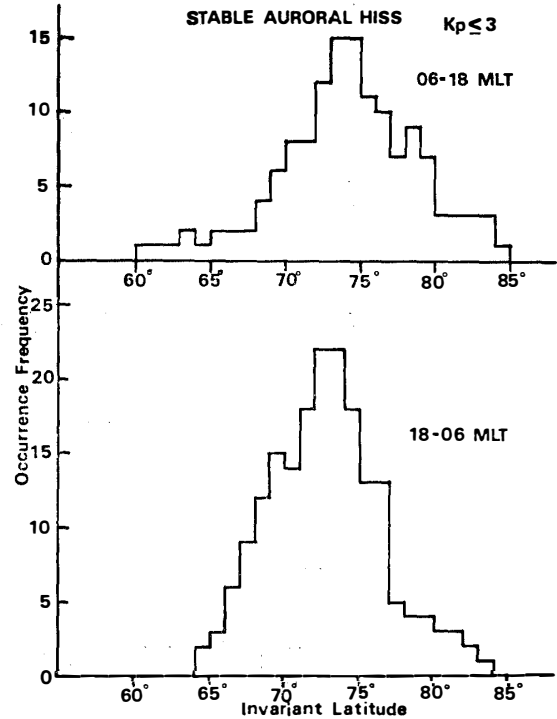


Fig. 9. Latitudinal distributions of the occurrence frequency of the stable auroral hiss in the daytime (06–18 MLT) and in the nighttime (18–06 MLT) for  $K_p \leq 3$ . The VLF data used were received from ISIS satellites at Syowa Station, Antarctica from January 1977 to February 1978.

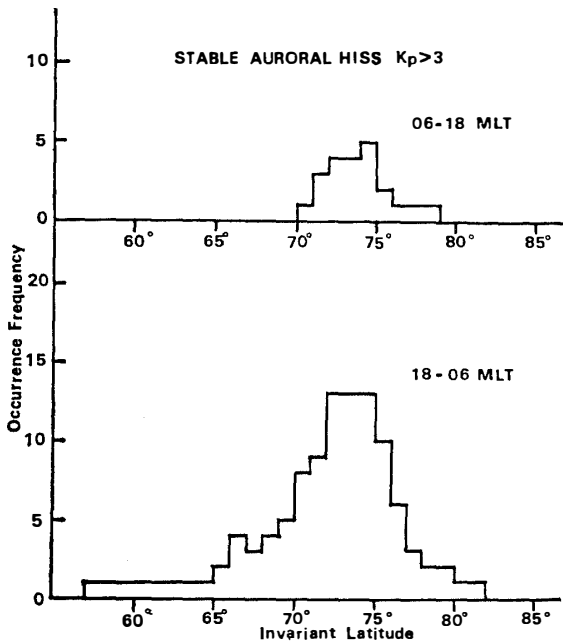


Fig. 10. Latitudinal distributions of the occurrence frequency of the stable auroral hiss in the daytime (06–18 MLT) and in the nighttime (18–06 MLT) for  $K_p > 3$ . The VLF data used were received from ISIS satellites at Syowa Station, Antarctica from January 1977 to February 1978.

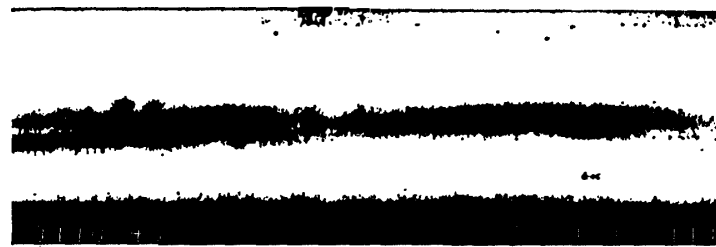
In summary, the latitudinal range of the frequent occurrence for the active auroral hiss agrees well with the usual auroral zone, while the latitudinal range of the stable auroral hiss zone is approximately the same at all local times. The stable hiss zone is, on the average, slightly higher than the active hiss zone in latitude during the nighttime and *vice versa* during the daytime. Hence, the active auroral hiss is caused by a structured flux of precipitating auroral electrons with energies near a few keV as previously pointed out from the *f-t* spectrum data of the auroral hiss.

WINNINGHAM and HEIKKILA (1974) have found a close association of the diffuse aurora with the polar rain of structureless and soft precipitating electrons with energies below 1 keV occurring over the polar cap region. The diffuse aurora is produced mainly by low-energy electrons with monotonous energy spectrum between about 100 eV and 10 keV. The observed electron energy spectrum in the diffuse aurora is generally composed of a background spectrum and a continuum spectrum, and the low-energy electrons have characteristics of the relative uniformity in the precipitation over a wide range of magnetic local time. The diffuse aurora can be identified as the optical image of the earthward termination of the plasma sheet at auroral altitudes (LUI *et al.*, 1977). The low-energy electrons, the so-called polar rain, producing the diffuse auroras seem to have similar characteristics to the stable auroral hiss in occurrence and in intensity variation.

### 5. Narrow-Band 5 kHz Hiss Observed in Mid-Latitude

Narrow-band 5 kHz hisses have been often observed at ground stations in mid- and low-latitudes (IWAI *et al.*, 1964; ONDOH and ISOZAKI, 1965, 1968) and it has been believed for about 15 years that the narrow-band 5 kHz hisses propagate in the earth-ionosphere wave guide from the auroral zone to low latitudes. However, we can not find any narrow-band 5 kHz hiss in VLF spectra observed by the polar orbiting satellites and also at auroral-zone ground stations.

Fig. 11a shows an example of the narrow-band 5 kHz hiss observed at invariant latitude  $61.1^\circ$  and at geomagnetic latitude  $55.4^\circ\text{S}$  on June 10, 1977 by ISIS-1. This hiss was received from ISIS-1 at Syowa Station, Antarctica. The narrow-band intensity data (Fig. 11b) clearly show the narrow-band 5 kHz hiss only in the 5 kHz band around invariant latitude  $61^\circ$ . Fig. 12 shows latitudinal variations of the occurrence frequency of the narrow-band 5 kHz hiss during the daytime and nighttime. These are derived from ISIS VLF data received at Syowa Station, Antarctica from February 1977 to January 1978. The narrow-band 5 kHz hiss occurs at almost invariant latitudes of  $61^\circ \pm 5^\circ$ , that are close to the average plasmopause latitude, although the occurrence frequency is higher for the nighttime than the daytime. The narrow-band 5 kHz hiss observed may propagate from the equatorial plasmopause, since the wave-particle interaction takes place preferentially around the equatorial plane (KENNEL and PETSCHER, 1966).



June 10, 1977 0111:00 UT Kp= 3  
 INV LAT 61.1° GM LT 0244  
 GM LAT -55.4° H 1956 km

Fig. 11a. Example of a narrow-band 5 kHz hiss observed at invariant latitude of 61.1° on June 10, 1977 ( $K_p=3$ ) by ISIS-1. The data used were received at Syowa Station, Antarctica.

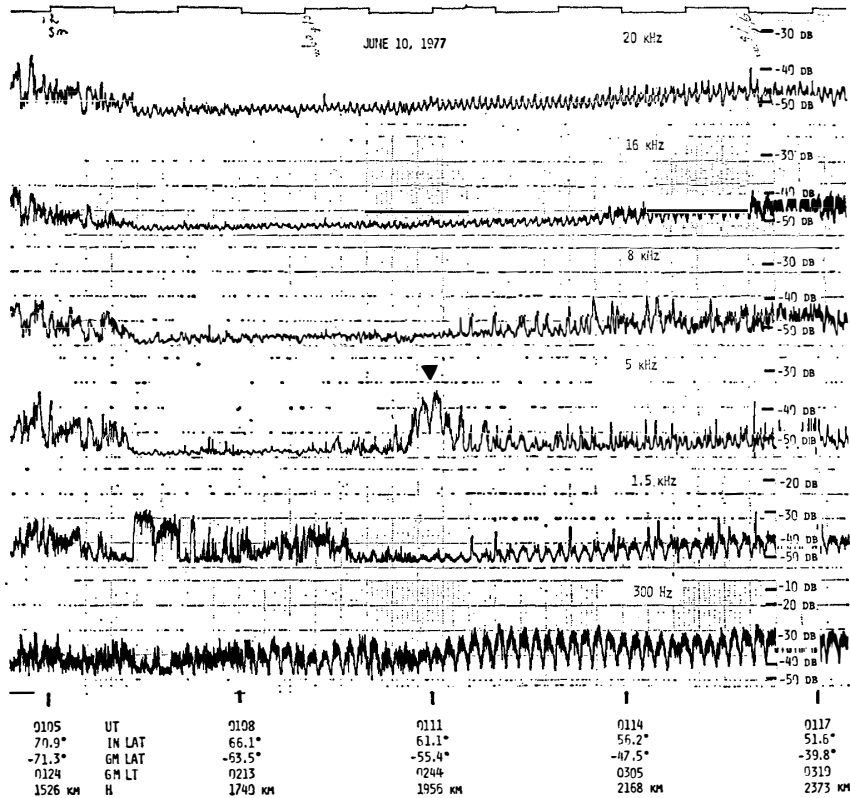


Fig. 11b. Narrow-band intensity data of the same ISIS pass as Fig. 11a. The intensity increase occurs clearly around 61° only in the 5 kHz band.

INAN and BELL (1977) have shown that the VLF rays starting close to the plasmapause are deflected inward by the negative plasmapause density gradients at low altitudes. The effective plasmapause guiding is only possible for rays injected at sufficiently low latitudes. This result suggests that the narrow-band 5 kHz hiss observed

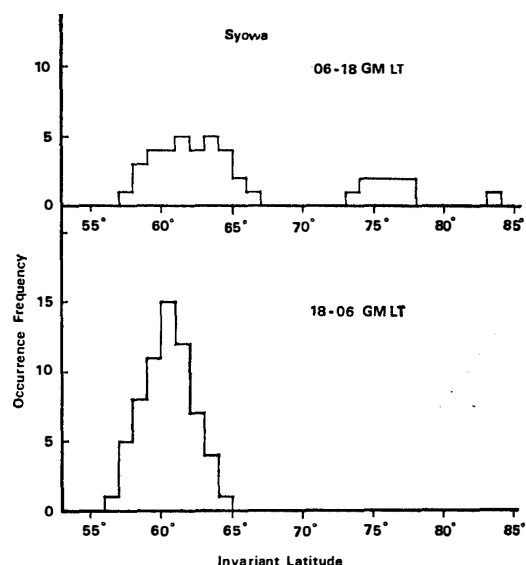


Fig. 12. Latitudinal distributions of the occurrence frequency of the narrow-band 5 kHz hisses in the daytime (06–18 MLT) and in the nighttime (18–06 MLT). The data used were received from ISIS satellites at Syowa Station, Antarctica from February 1977 to January 1978.

around  $61^\circ$  in the topside ionosphere is generated around the equatorial plasmopause. The precipitating electrons with energy above 10 keV were observed outside the plasmopause in geomagnetically quiet and disturbed conditions (HULTQVIST, 1975). The OGO results also show the equatorial electron ( $> 36$  keV) fluxes of  $10^7$ – $10^8/\text{cm}^2\cdot\text{s}$  for  $L=3.5$ – $4.5$  outside the plasmopause (VETTE, 1972). Thus, the narrow-band 5 kHz hiss seems to be generated by the cyclotron instabilities of energetic electrons in the vicinity of the equatorial plasmopause.

The parallel resonant energy  $E_r$  of electrons resonating with the whistler mode waves ( $f$ ) is given by  $E_r = f_H / [f(1 - f/f_H)^2] \cdot B^2 / 2\mu N$ , where  $f_H$  denotes the electron gyrofrequency,  $N$  the electron density ( $\text{m}^{-3}$ ),  $B$  the geomagnetic field flux density (1 gauss =  $10^{-4}$  wb/m $^2$ ) and  $\mu = 1.26 \times 10^{-6}$  H/m (KENNEL and PETSCHKE, 1966). Table 1 gives the parallel energies of electrons resonating with the 5 kHz whistler-mode waves calculated for appropriate parameters in the vicinity of the equatorial plasmopause.

Table 1. Parallel resonant energies of electrons resonating with 5 kHz whistler mode waves in the equatorial plane.

Location	$f_H$ kHz	$B$ wb/m $^2$	$N/\text{cm}^3$	$E_r$
Outside the plasmopause	11.6	$4.16 \times 10^{-7}$	1	190 keV
$A=61^\circ, L=4.25$			10	19 keV
Plasmopause	13.6	$4.84 \times 10^{-7}$	10	40 keV
$A=60^\circ, L=4.00$			$10^2$	4 keV
Inside the plasmopause	19.2	$6.86 \times 10^{-7}$	$10^3$	1.8 keV
$A=58^\circ, L=3.56$			$10^4$	180 eV

$A$ : Geomagnetic invariant latitude

Hence, the narrow-band 5 kHz hiss seems to be generated by the cyclotron instabilities of several keV—a few tens keV electrons for the most feasible ambient electron density of  $10/\text{cm}^3$ — $10^3/\text{cm}^3$  in the vicinity of the equatorial plasmopause.

The narrow-band 5 kHz hiss generated near the equatorial plasmopause will propagate towards the ionosphere along the plasmopause field line, and then it will propagate towards mid- and low-latitudes *via* the earth-ionosphere wave guide mode after penetrating through the ionosphere around the plasmopause latitude.

## 6. Conclusions

We have analyzed the ISIS VLF electric field data received at Syowa Station, Antarctica. The source altitude of VLF saucers is estimated at less than about 800 km below the ISIS satellites by assuming the limiting ray model for the VLF saucer. It has been remarked that VLF saucers occur often around the high- and low-latitude ends of the auroral hiss region.

The wide-band auroral hisses have been classified into the active auroral hiss and the stable auroral hiss according to the time variation of the narrow-band intensity data processed from the wide-band tapes of the ISIS VLF data. The stable auroral hiss usually occurs on the higher latitude side of the active auroral hiss. The occurrence zone of active auroral hiss coincides well with the usual auroral zone, while the stable auroral hiss zone lies in invariant latitudes from about  $80^\circ$  to about  $70^\circ$  during the daytime and nighttime. Morphological comparisons have been made between the active hiss and the polar showers or squalls and between the stable hiss and the polar rain producing the diffuse aurora.

Finally, the narrow-band 5 kHz hiss has been statistically found around invariant latitude of  $61^\circ$  at all local times from ISIS VLF data received at Syowa Station, Antarctica, and the generation of narrow-band 5 kHz hiss has been discussed in terms of the cyclotron instabilities of electrons with energies from a few tens keV to several keV in the vicinity of the equatorial plasmopause.

## Acknowledgments

We are grateful to Dr. R. E. BARRINGTON, Communications Research Centre, Canada, NASA, U. S. A. and the ISIS Working Group for their support to the ISIS VLF observation at Syowa Station, Antarctica. We also thank the members of the 18th wintering party of the Japanese Antarctic Research Expedition at Syowa Station for their collaboration in data acquisition.

## References

- BARRINGTON, R. E. (1969): Ionospheric ion composition deduced from VLF observations. Proc. IEEE, **57**, 1036–1053.

- FRANK, L. A. and ACKERSON, K. L. (1972): Local-time survey of plasma at low altitudes over the auroral zone. *J. Geophys. Res.*, **77**, 4116–4127.
- GURNETT, D. A. (1978): Electromagnetic plasma wave emissions from the auroral field lines. *J. Geomagn. Geoelectr.*, **30**, 257–272.
- HUGHES, A. R. W., KAISER, T. R. and BULLOUGH, K. (1971): The frequency of occurrence of VLF radio emissions at high latitudes. *COSPAR Space Research XI*, ed. by K. YA. KONDRATYEV *et al.* Berlin, Akademie-Verlag, 1323–1330.
- HULTQVIST, B. (1975): The ring current and particle precipitation near the plasmapause. *Ann. Géophys.*, **31**, 111–126.
- INAN, U. S. and BELL, T. F. (1977): The plasmapause as a VLF wave guide. *J. Geophys. Res.*, **82**, 2819–2827.
- IWAI, A., OHTSU, J. and TANAKA, Y. (1964): The observation of VLF emissions at Moshiri. *Proc. Res. Inst. Atmos., Nagoya Univ.*, **11**, 29–40.
- JAMES, H. G. (1976): VLF saucers. *J. Geophys. Res.*, **81**, 501–514.
- KENNEL, C. F. and PETSCHER, H. E. (1966): Limit on stably trapped particle fluxes. *J. Geophys. Res.*, **71**, 1–28.
- LUI, A. T. Y., VENKATESAN, D., ANGER, C. D., AKASOFU, S.-I., HEIKKILA, W. J., WINNINGHAM, J. D. and BURROWS, J. R. (1977): Simultaneous observations of particle precipitations and auroral emissions by the ISIS 2 satellite in the 19–24 MLT sector. *J. Geophys. Res.*, **82**, 2210–2226.
- MOSIER, S. R. and GURNETT, D. A. (1969): VLF measurements of the Poynting flux along the geomagnetic field with the Injun-5 satellite. *J. Geophys. Res.*, **74**, 5675–5687.
- MOSIER, S. R. and GURNETT, D. A. (1972): Observed correlations between auroral and VLF emissions. *J. Geophys. Res.*, **77**, 1137–1145.
- ONDOH, T. and ISOZAKI, S. (1965): Observation of VLF hiss at Hiraio, Japan. *Rep. Ionos. Space Res. Jpn*, **19**, 225–230.
- ONDOH, T. and ISOZAKI, S. (1968): Characteristics of low-latitude VLF emissions. *J. Radio Res. Labs.*, **15**, 133–146.
- OZAKI, T., IWASE, M., YOSHINO, T., MATSUO, T. and FUKUNISHI, H. (1979): ISIS-1–2 de kansoku sareta VLF-sôsa no tokusei (Characteristics of VLF saucers observed by ISIS-1, -2 satellites). *Nankyoku Shiryo* (Antarct. Rec.), **64**, 167–178.
- STIX, T. H. (1962): *The Theory of Plasma Waves*. New York, McGraw-Hill, 14 p.
- TAYLOR, W. W. L. and GURNETT, D. A. (1968): Morphology of VLF emissions observed with the Injun 3 satellite. *J. Geophys. Res.*, **73**, 5615–5626.
- TEMERIN, M. (1979): A comment of the source region of VLF saucers. *J. Geophys. Res.*, **84**, 6691–6693.
- VETTE, J. I. (1972): Magnetospheric particle populations. *Earth's Magnetospheric Processes*, ed. by B. M. McCORMAC. Dordrecht, D. Reidel, 53–67.
- WINNINGHAM, J. D. and HEIKKILA, W. J. (1974): Polar cap auroral electron fluxes observed with ISIS-1. *J. Geophys. Res.*, **79**, 949–957.

(Received June 30, 1980)